# Semiconducting Mixed Valence Sulfido (Selenido) Ferrates: Optical, Dielectric, and Electrochemical Impedance Properties

M. Reza Ghazanfari,[a] Lara Janus,[a, b] Islam Ramadan,[a] Mirko Tallu,[c] Stefanie Dehnen,[c] and Günther Thiele*[a, d]
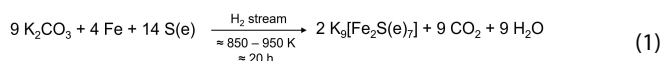
The ternary potassium sulfido and selenido ferrates $K_9[Fe_2S(e)_7]$ were synthesized as pure phases through a facile and straightforward solid-state method. The compounds crystalize isotypic as has been reported previously. UV-visible measurements indicate semiconductivity, showing direct optical band gaps with energies of 1.91 eV for the sulfido and 1.72 eV for the selenido ferrate. Investigations of dielectric and impedance properties provide their dielectric constants in the range of 60 to 74 at room temperature at a frequency of 1 kHz, as well as ionic conductivity values in the range of $2.08 \cdot 10^{-5}$ and $2.61 \cdot 10^{-5}$ mS cm$^{-1}$. Both, the dielectric constants and the calculated ionic conductivity of the selenido ferrate are higher compared to the sulfido ferrate, corresponding to the larger unit cell volume and increased bond lengths in the selenido ferrates. The dielectric constants are comparably higher than the reference material of $SiO_2$, which might introduce them for dielectric applications.

## Introduction

Mixed valence materials such as metal oxides, metal sulfides, and metalates can show a wide range of properties impacted by the coexistence of transition metals with different nominal oxidation states.[1] Iron can be incorporated in different compounds with a wide range of oxidation states, e.g., $+1$, $+4$, $+5$, $+6$, and $+7$,[2] however the most common oxidation states, particularly in mixed valence materials are $+2$ and $+3$.[3,4] There are several mixed valence compounds containing iron (II) and (III) such as ferrites and ferrates. Among ferrites, magnetite with the chemical composition of $Fe^{+2}Fe^{+3}_2O_4$ is most likely the best-known compound, especially due to its unique magnetic properties.[5,6] Within these materials, iron (II) ions can often be substituted with other $3d$ transition metals, such as, Mn, Co,

and Ni.[7] Alkali metal ferrates including oxido, sulfido, and selenido ferrates show a few mixed valence compounds, such as, $K_3[Fe_2O_4]$, $K_3[Fe_2S_4]$, $K_3[Fe_2Se_4]$, $Na_3[Fe_2S_4]$, $K[Fe_2Se_3]$, $K_9[Fe_2S_7]$ (**1**), and $K_9[Fe_2Se_7]$ (**2**), although their magnetic, electrical, and optical properties are rarely reported.[8–12] For instance, $K_3[Fe_2S_4]$ displays a high dielectric constant in the range of benchmark dielectric materials, mid-range electrochemical impedance values, and an antiferromagnetic structure with a high magnetization which results from magnetic exchange interaction between iron ions with different oxidation states of $+2$ and $+3$.[4] Although the crystal structure and magnetic properties of $K_9[Fe_2S_7]$, (**1**), and $K_9[Fe_2Se_7]$, (**2**), are already reported,[12] their electrical properties, including dielectric and impedance features, are still unknown. **1** and **2** were synthesized for the first time in 1993 by Bronger and Ruschewitz along with the analogous compounds of the other alkali metals (Rb and Cs).[12] **1** and **2** were reportedly obtained by heating the stoichiometric mixture of potassium carbonate, elemental iron and chalcogen (S or Se) at 850 to 950 K for around 20 hours in a stream of hydrogen gas, according to the following reaction equation:

$$9\ K_2CO_3 + 4\ Fe + 14\ S(e) \xrightarrow[\approx 850 - 950\ K]{\substack{H_2\ \text{stream} \\ \approx 20\ h}} 2\ K_9[Fe_2S(e)_7] + 9\ CO_2 + 9\ H_2O \tag{1}$$

The exact amount of starting materials, reaction yield, and purity of the products were not reported. **1** and **2** are isotypic and crystalize in the cubic space group type $P2_13$ (198) with four chemical formula moieties per cell ($Z = 4$). The cell parameters of $a = b = c = 12.663(1)$ Å and $a = b = c = 13.118(1)$ Å are reported at room temperature for **1** and **2**, respectively.[12] Red color of **1** and black color of **2** were reported, while both are extremely sensitive to air and moisture.[12] Excerpts of the crystal structure are depicted in Figure 1. In both compounds, the anionic sublattice contains isolated polyhedra. $Fe^{2+}$ ions are

[a] Dr. M. Reza Ghazanfari, M. Sc. L. Janus, M. Sc. I. Ramadan, Dr. G. Thiele
Fachbereich Biologie, Chemie, Pharmazie, Freie Universität Berlin, Fabeckstr. 34–36, 14195 Berlin, Germany
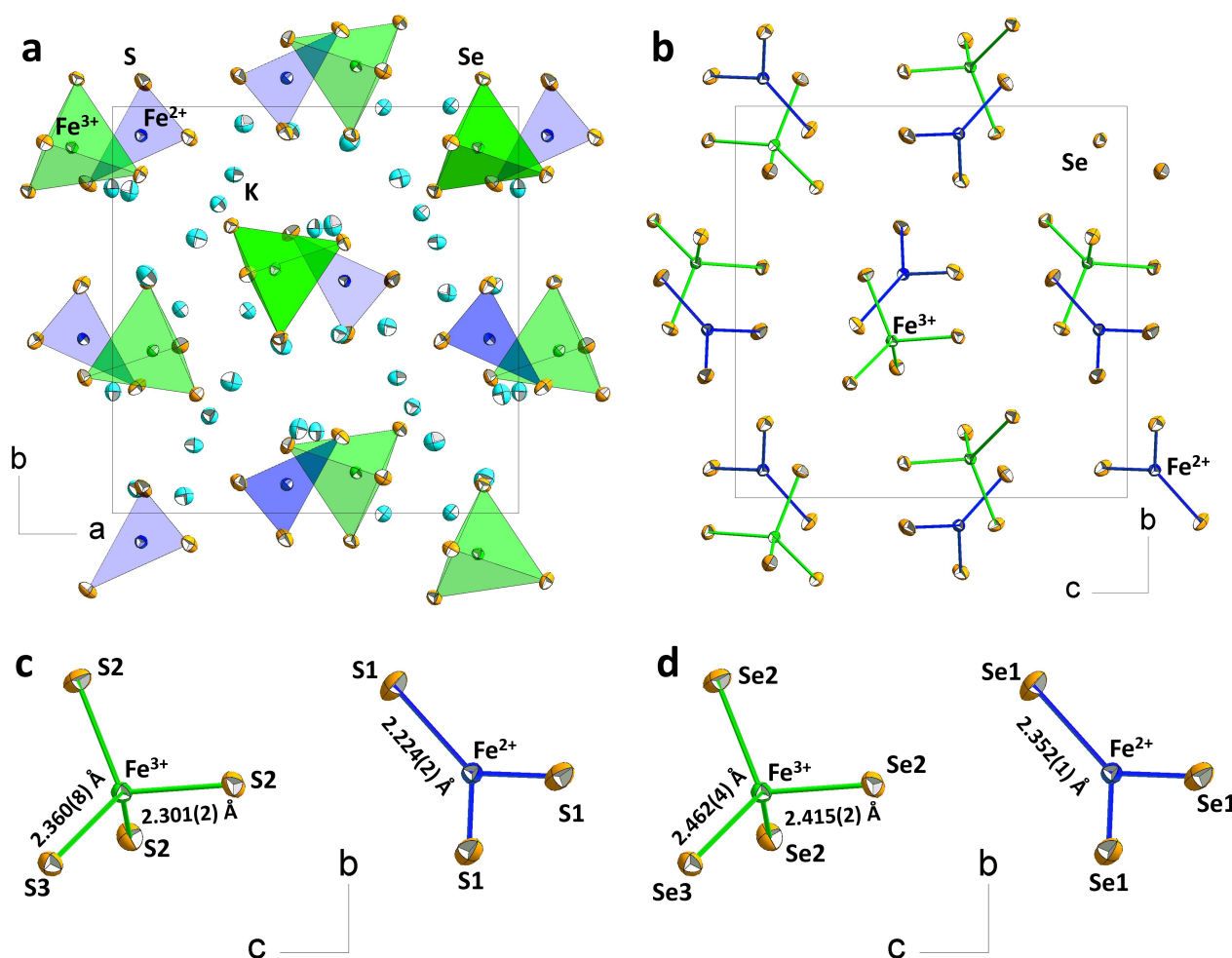E-mail: guenther.thiele@fu-berlin.de

[b] M. Sc. L. Janus
Department of Materials and Environmental Chemistry, Stockholm University, SE-114 18 Stockholm, Sweden

[c] M. Sc. M. Tallu, Prof. Dr. S. Dehnen
Institute of Nanotechnology (INT), Karlsruhe Institute of Technology (KIT), Kaiserstr. 12, 76131 Karlsruhe, Germany

[d] Dr. G. Thiele
Institut für Anorganische und Analytische Chemie, Albert-Ludwigs-Universität Freiburg, Albertstr. 12, 79104 Freiburg, Germany

**EurJIC**
European Journal of Inorganic Chemistry

Research Article
**doi.org/10.1002/ejic.202400522**

Chemistry
Europe
European Chemical
Societies Publishing

**Figure 1.** Excerpts of the crystal structure of **2**, isotypic to **1**. (a) **2** depicted along the *c*-axis, indicating isolated polyhedra. (b) **2** depicted along the *a*-axis, indicating trigonal coordination of $Fe^{2+}$ and tetragonal coordination of $Fe^{3+}$ ions by sulfurs. (c) ORTEP diagram of the $Fe^{2+}$ and $Fe^{3+}$ coordination in **1** depicted along the *a*-axis according to the reported bond lengths in literature,[12] displaying a slight distortion in the tetrahedra of $[Fe^{3+}S_4]^{5-}$. (d) ORTEP diagram of the $Fe^{2+}$ and $Fe^{3+}$ coordination in **2** depicted along the *a*-axis, displaying larger differences in bond lengths in the $[Fe^{3+}Se_4]^{5-}$ tetrahedra.

coordinated in trigonal planar units of $[Fe^{2+}S(e)_3]^{4-}$ and $Fe^{3+}$ ions are coordinated tetrahedrally as $[Fe^{3+}S(e)_4]^{5-}$ units (Figure 1a and b). The Fe—S bond lengths within the tetrahedra are different, indicating a slight distortion along the [111] directions (Figure 1c). The observed distortion in **2** is larger than in **1**, due to the longer iron-chalcogen bond lengths in **2** compared to **1** (Figure 1d).

In addition to the crystal structures, the magnetic properties of **1** and **2** are already studied, reporting an antiferromagnetic order with high spin states for both $Fe^{2+}$ and $Fe^{3+}$.[12] In some mixed valence chalcogenido ferrates, such as $K_3[Fe_2S_4]$, with a strand-like anionic sublattice, the iron ions with different oxidation states occupy the same position in the crystal structure which makes them and their individual impacts on physical properties indistinguishable.[4] In contrast, in both **1** and **2**, $Fe^{2+}$ and $Fe^{3+}$ ions occupy different structural positions with different coordination geometries. These differences encouraged us to investigate their hitherto unreported properties.
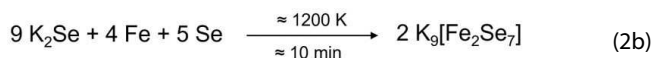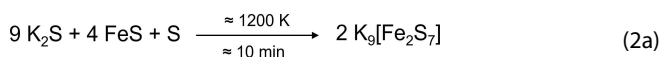
Here we report the bulk synthesis of both **1** and **2**, via a straightforward and comparably time-effective method, as well as investigation of their optical, dielectric, and electrochemical impedance properties, which are still unknown according to the best of our knowledge. We also report on the low temperature single crystal structure determination of **2**, indicating no phase transformation and solely temperature induced reduction of the unit cell parameters and respective bond lengths.

## Results and Discussion

### Synthesis and Structural properties

**1** was synthesized by fusing the stoichiometric mixture of $K_2S$, FeS, and elemental sulfur as starting materials at around 1200 K for approx. 10 minutes under inert atmosphere in a fused silica ampule, according to Equation (2a). To synthesize **2**, a mixture

**EurJIC**
European Journal of Inorganic Chemistry

Research Article
doi.org/10.1002/ejic.202400522

Chemistry
Europe
European Chemical
Societies Publishing

of $K_2Se$, elemental iron, and selenium were mixed, and heat treated in the same approach, according to Equation (2b).

$$9\ K_2S + 4\ FeS + S \xrightarrow[\approx 10\ min]{\approx 1200\ K} 2\ K_9[Fe_2S_7] \tag{2a}$$

$$9\ K_2Se + 4\ Fe + 5\ Se \xrightarrow[\approx 10\ min]{\approx 1200\ K} 2\ K_9[Fe_2Se_7] \tag{2b}$$

To synthesize **1** and **2**, $K_2S(e)$ can be heat-treated either with binary FeS(e) or a mixture of Fe and S(e). The usage of binary starting materials instead of elemental precursors avoids the exothermic and comparably harsh intermediate reaction of iron with the chalcogen. However, for synthesizing **2**, the significantly reduced prices for Fe and Se compared to FeSe led us to employ the elements. In contrast to the literature-reported method which needed around 20 hours heating under a stream of hydrogen, followed by a cooling period, both **1** and **2** were produced according to the present technique within minutes. The reactions yielded 9.41 g (94% yield) of dark red powder of **1** and 9.15 g (91% yield) of shiny dark brown powder of **2**, respectively. The reaction can be scaled only limited by the size of the reaction vessel. Single crystals of **2** were obtained through a solvothermal treatment by heating the as-synthesized powders in pyridine at 423 K for 48 hours. Similar attempts to isolate single crystals of **1** suitable for X-ray diffraction analysis yielded heavily twinned species that resulted in datasets of insufficient quality for publication in all cases. However, obtained unit cell parameters: $a = b = c = 12.663(1)$ Å, $\alpha = \beta = \gamma = 90°$, V = 2030.53 Å³,[12] and initial structure solution indicates the presence of **1** (tentative space group type: $P2_13$), also at 100 K. We note in passing that the low-temperature measurements indicate partial disorder of $[FeS_3]$ and $[FeS_4]$ units, as well as corresponding split positions of the surrounding potassium ions. Due to the present twinning and resulting data quality, different approaches for crystallization will be needed to make conclusive statements.

The cell parameters of synthesized **2**, measured at 100 K, are $a = b = c = 13.0419(13)$ Å, $\alpha = \beta = \gamma = 90°$, V = 2218.3(7) Å³ with the bond lengths of $Fe^{2+}-Se$ equals to 2.352(1) Å, while the bond lengths of $Fe^{3+}-Se$ are in the range of 2.415(2) Å and 2.462(4) Å.

The literature reported cell parameters of **2**, measured at room temperature, are $a = b = c = 13.118(1)$ Å, $\alpha = \beta = \gamma = 90°$, V = 2257.37 Å³, with the iron–chalcogen bond lengths equals to be 2.359(5) Å ($Fe^{2+}-Se$, and $Fe^{3+}-Se$ are in the range of 2.416(5) Å and 2.472(5) Å.[12] The observed differences in the cell parameters and bond lengths can be explained by the different measurement temperatures in the current study (100 K) and the reported work (room temperature). Further details on the single crystal measurements, the refinement details, and obtained structural parameters are provided in the Supplementary Information (SI) file.

According to the results of powder X-ray diffraction (P-XRD) measured at room temperature, both **1** and **2** are confirmed isotypic and in the literature-reported space group type $P2_13$ (198).[12] The phase purity of as-synthesized **1** and **2** was evaluated by Rietveld structure refinements of the powder X-ray diffraction (PXRD) results, shown in Figure 2. The overall signal to noise ratio is comparably low and impacted by limited measurement time due to sensitivity, as well as potential amorphous phases and/or X-ray fluorescence. Accordingly, the absence of additional reflections of impurities can only serve as an approximation, whilst Rietveld refinement for both compounds indicate phase purity with a crystallinity degree of 94% ±3% and 96% ±3% for **1** and **2**, respectively. The results of the energy dispersive X-ray (EDX) spectroscopy (Figure S1) show the elemental composition of the compounds of the expected stoichiometric ratio (9:2:7), pointing towards the absence of significant (amorphous) side products.
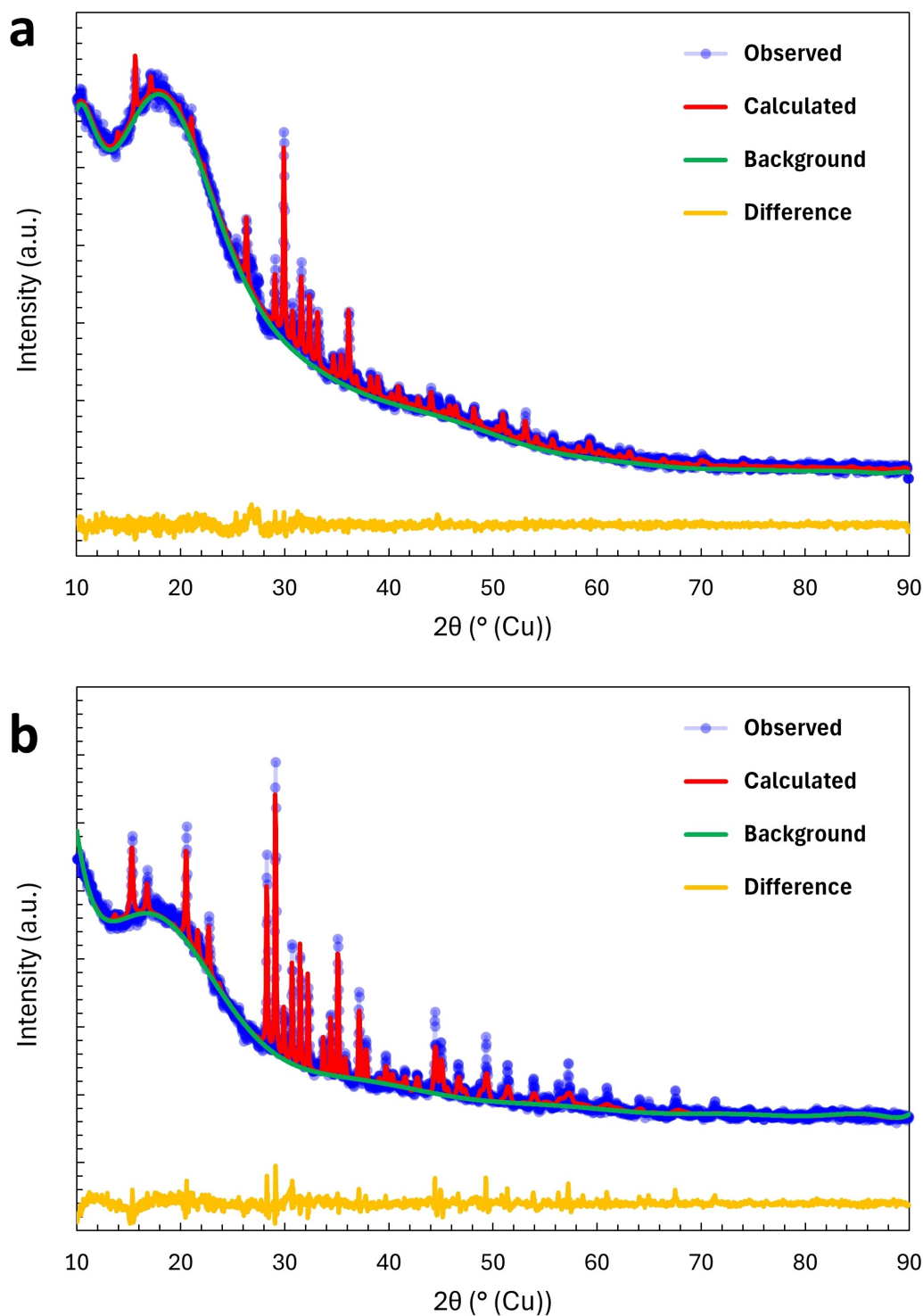
## Optical and Electrical Properties

The optical absorption properties of **1** and **2** were investigated by solid state UV-visible reflectance measurements. Figure 3 displays the Tauc plots calculated by applying the Kubelka-Munk function[13] on the UV-visible spectroscopy results. Accordingly, the optical band gap values are around 1.91 eV for **1** and around 1.72 eV for **2**, which are in a good agreement with their colors. The Tauc plots point towards direct band gaps for both compounds. Minor additional signals in both graphs indicate further *d-d* transitions, however, the very low intensities prevent extensive discussion or precise assignment.

Bulk pellets of **1** and **2** were sintered at 723 K for 18 hours, followed by dielectric and electrochemical impedance measurements. The dielectric constant was calculated using the measured capacitance values of the pellets, according to Equation (3).[14]

$$\kappa = C \cdot d \cdot \varepsilon_0^{-1} \cdot A^{-1} \tag{3}$$

Where $\kappa$, $C$, $d$, $\varepsilon_0$, and $A$ are the dielectric constant, the measured capacitance, the thickness of the pellets, the dielectric constant value of free space equal to $8.85 \cdot 10^{-12}\ m^{-3}kg^{-1}s^4A^2$, and the contact surface of the pellets, respectively. Figure 4a indicates the results of dielectric measurements for **1** (in red) and **2** (in blue). The curves of dielectric constants as a function of frequency, in the range of 20 Hz to 1 MHz, are plotted in the main frame.
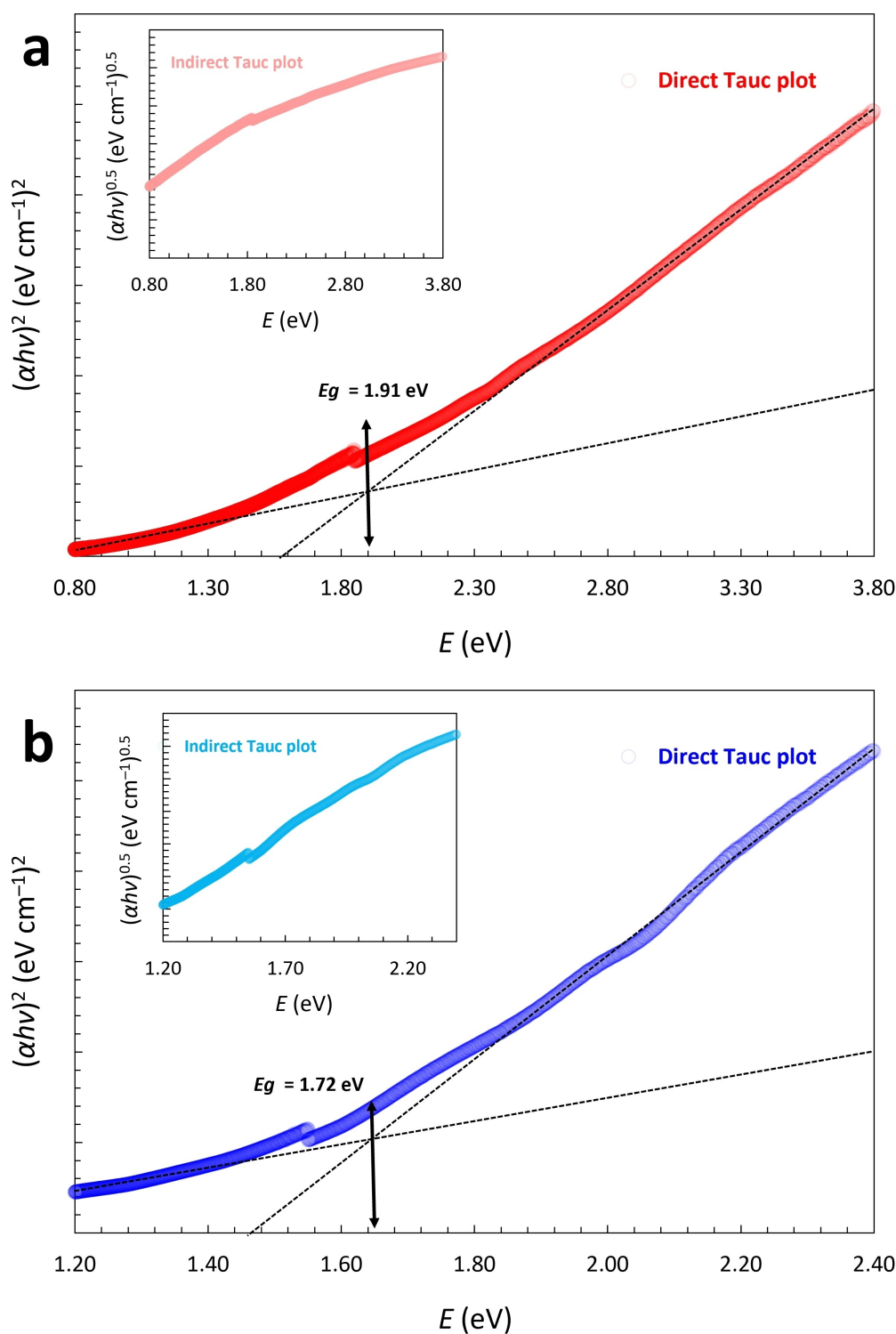
In both materials, the observed dielectric constants are decreased by increasing the measurement frequency. Whilst the decrease rate is initially high and then gradually decreases at frequencies around 1 kHz. This change can be explained by a gradual deactivation of the space charge polarization, as a dominant polarization mechanism at low frequencies up to approx. 1 kHz.[14] The comparison of the dielectric constant values of **1** and **2** shows the higher constants for **2**, which can be attributed to the slightly larger size of the selenium ions compared to the sulfur ions. The comparably larger cells of **2** might introduce larger polarization areas, resulting in stronger polarization mechanisms. The impact of the bond lengths and unit cell size on the dielectric properties are occasionally reported for a few different systems such as $Sb_2Se_2S$,[15] $CsPbX_3$

**Figure 2.** (a) Rietveld refinement of the PXRD results of as-synthesized **1**. (b) Rietveld refinement of the PXRD results of as-synthesized **2**.

(X=Cl, Br, I),[16] and $Be_xMg_{1-x}O$ (x < 0.5).[17] The dielectric constant values of **1** and **2** at room temperature and a frequency of 1 kHz are 60.98 and 73.49, respectively. These values are higher than the dielectric constant of the standard reference material, $SiO_2$: 3.6–3.9 at 1 kHz,[18] which can potentially introduce the title compounds for applications as gate materials in analogy to metal–oxide–semiconductor field-effect transistor (MOSFET) technologies and electrical circuits.[18] However, compared to the dielectric constants of the common capacitor dielectric materials, such as, barium and strontium titanates, the values of **1** and **2** are significantly lower, which will limit their applicability as circuit capacitors.[19] The dielectric constant values depend on
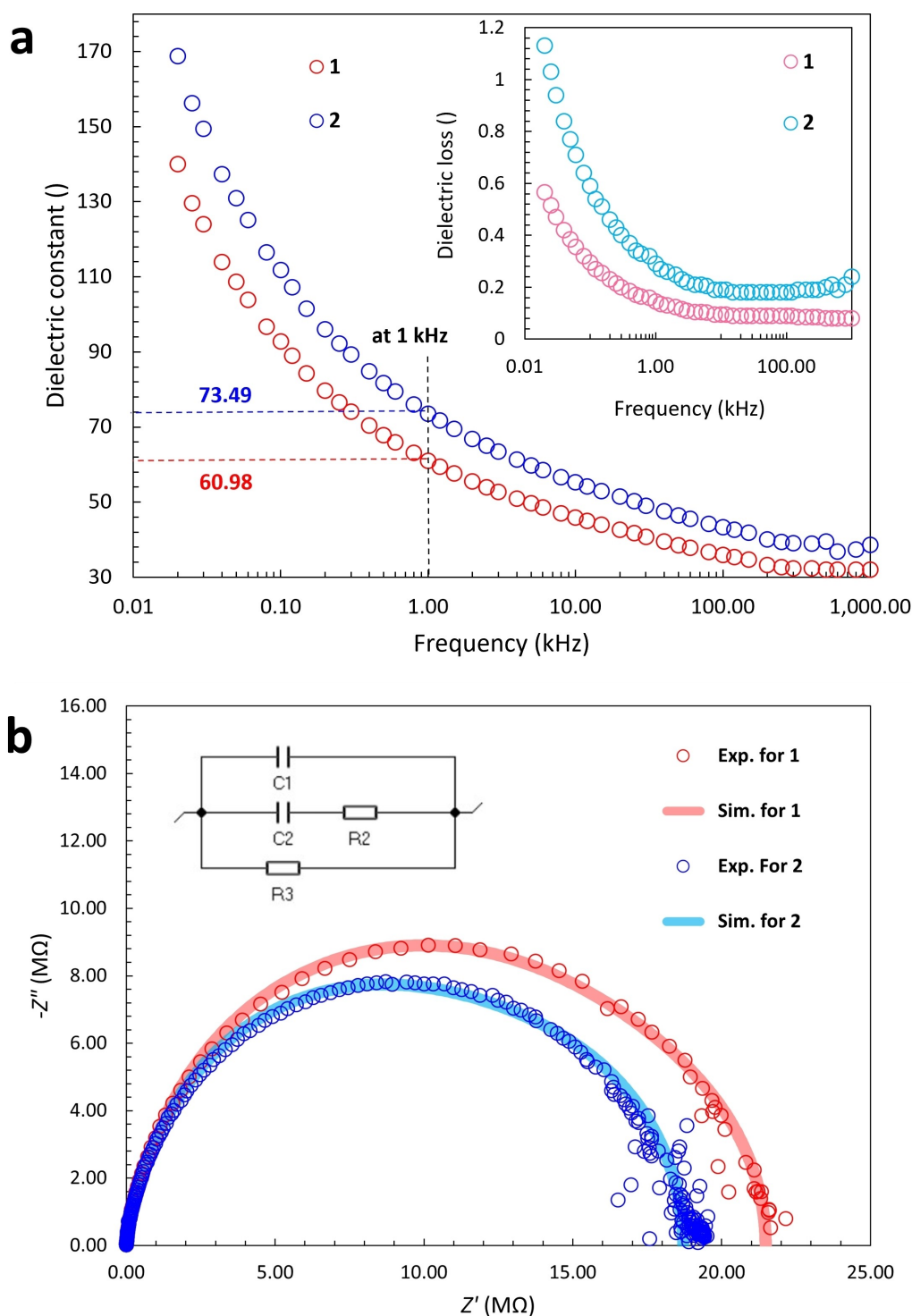
**Figure 3.** (a) Direct Tauc plot of **1** calculated using UV-visible measurement, indicating a band gap of 1.91 eV. (Inset) Indirect Tauc plot of **1** without any intersection with the abscissa. (b) Direct Tauc plot of **2** calculated using UV-visible measurement, indicating a band gap of 1.72 eV. (Inset) Indirect Tauc plot of **2** without any intersection with the abscissa.

different parameters such as crystallinity degree, bond length and ionicity, and lattice symmetry which can directly impact on the polarization ability of materials.[19] **1** and **2** crystalize in the chiral space group of $P2_13$, however it is not polar. The $P2_13$ space group does not support a spontaneous electric dipole moment because it lacks a polar axis. Although it is chiral due to the absence of inversion symmetry, its high degree of rotational symmetry, characteristic of the cubic system, pre-

**EurJIC**
European Journal of Inorganic Chemistry

Research Article
doi.org/10.1002/ejic.202400522

**Chemistry Europe**
European Chemical
Societies Publishing

**Figure 4.** (a) Dielectric constant variations of **1** and **2** as a function of the measurement frequency at room temperature. (Inset) Dielectric loss values of **1** and **2** as a function of the measurement frequency at room temperature. (b) Nyquist plots of **1** and **2**, indicating semicircular arcs for both compounds measured at room temperature. (Inset) Equivalent circuit designed for simulating complex impedance plots.

vents the formation of the net dipole necessary for ferroelectricity.[15–17] Thus, they can be considered as paraelectric materials, showing significantly lower dielectric constant values compared to the ferroelectric materials with a polar non-

centrosymmetric crystal structures such as barium titanates.[19] Since relatively high charges are concentrated on the anions, strong ionic interactions occur, which potentially reduce the ion mobility. Additionally, there are neither suitable voids nor

**EurJIC**
European Journal of Inorganic Chemistry

Research Article
**doi.org/10.1002/ejic.202400522**

**Chemistry Europe**
European Chemical Societies Publishing

sufficient defects to facilitate high ionic mobility. As a result, the contribution of the space charge mechanism is low, leading to reduced dielectric constants and higher resistance.

The dielectric loss values of **1** and **2** as a function of the measurement frequency are plotted in the inset frame of Figure 4a. For both samples, the dielectric loss values are gradually decreased by increasing the frequency, in a similar trend as the dielectric constant variations. At a frequency of 1 kHz, the dielectric loss values are 0.12 for **1** and 0.27 for **2**. The comparably high values of dielectric losses can be considered as another obstacle to their use in circuit capacitor applications.[20] For **1**, at a frequency of 10 kHz the dielectric loss values decrease to lower than 0.01, as an acceptable limit in common applications, and the dielectric constant is around 45.

Figure 4b displays the Nyquist plots of **1** and **2**, indicating the complex impedance values measured at room temperature and in the frequency range of 100 mHz to 1 MHz. For both compounds, the complex impedance plots trend semi-circularly, demonstrating ionic conductivity behaviors of the samples. However, in both cases there is no tail in the post-intersect region of the semicircular arcs. The lack of clear tails in these plots indicates a possible contribution of the electronic conductivity (electronic leakage) in the calculated electrical conductivity values. The semicircular arc typically represents the bulk properties of the material, combining the resistance and capacitance of the bulk phase.[22] The absence of a tail indicates that the bulk properties dominate and the electrode or inter-face properties (which usually show up as a tail) are minimal or negligible in this measurement. This could be due to a highly conductive interface or minimal impedance from interfacial layers. The semicircular arc without a tail suggests that the bulk properties are predominant, with minimal interfacial impedance or that the measurement range did not capture low-frequency effects adequately. Further investigation with extended fre-quency ranges or additional electrochemical techniques might provide more insights into the interfacial properties and potential leakage paths.[22] According to the experimental results, the complex impedance curves were simulated by designing the equivalent circuits (inset of Figure 4b). Whilst the experimentally measured Nyquist plots show a single arc, the equivalent circuit was designed according to the one-arc model including a capacitance (C1) element in parallel with a series of resistance (R2) and capacitance (C2) elements for the bulk sample.[21] An additional resistance (R3) element was designed in the equivalent circuit to represent the possible electronic leakage of the bulk sample.[21]

For both **1** and **2**, the simulated plots were calculated based on the same equivalent circuit. In both cases, the simulated trends are in good agreement with the experimental results. The values of the real parts of impedance ($Z'$) at the intersect points of the complex impedance arcs with the abscissa are considered as bulk resistivity values which are 21.48 and 19.12 $\Omega$ for **1** and **2**, respectively.

The corresponding ionic conductivity values were calculated according to the Nyquist equation as follows:[23]

$$IC = dR_b^{-1} \ A^{-1} \tag{4}$$

Where *IC* is the ionic conductivity, *d* is the thickness of the pellet, *A* is the contact area of the pellet, and $R_b$ is the bulk resistivity extracted from the Nyquist plot. The calculated ionic conductivity values are $2.08 \cdot 10^{-5}$ mS cm$^{-1}$ and $2.61 \cdot 10^{-5}$ mS cm$^{-1}$ for **1** and **2**, respectively. The higher value of **2** might be explained by its larger cell parameters as well as longer bond lengths of selenium ions compared to the sulfur ions, which can potentially increase the mobility of the potassium ions. The enhancing impact of longer bond length on the ionic conductivity is already reported for sulfur and selenium containing materials,[24,25] whilst the substitution of sulfur with selenium can broaden the ion migration channels and create a softer nature of the lattices.[26]

However, these values are not comparable to the values reported for other potassium-containing superionic conducting materials (1 to 35 mS cm$^{-1}$).[27] The very low measured values of the ionic conductivity of the title compounds are expected due to the isolated nature of the anionic moieties.

## Conclusions

We present the multigram synthesis of pure K$_9$[Fe$_2$S$_7$] and K$_9$[Fe$_2$Se$_7$] via a straightforward technique. The compounds crystallize isotypic in the literature reported space group type $P2_13$ (198). The obtained single crystals and powders were structurally and microstructurally characterized using XRD and EDX methods. The optical, dielectric, and electrochemical impedance properties of both compounds are investigated for the first time. Tauc plots calculated based on the UV-visible measurements indicate the direct optical band gaps with energies of around 1.91 and 1.72 eV for K$_9$[Fe$_2$S$_7$] and K$_9$[Fe$_2$Se$_7$], respectively. The measurements reveal the electrical properties of both compounds with the dielectric constant values of 60.98 for K$_9$[Fe$_2$S$_7$] and 70.49 for K$_9$[Fe$_2$Se$_7$] at room temperature at 1 kHz, which are considerably higher than of reference SiO$_2$ but well below titanate materials. According to the electrochemical impedance measurements, both compounds show ionic con-ductivities in the order of $10^{-5}$ mS cm$^{-1}$, which is significantly below the suitable range of potassium-containing superionic conducting materials.

## Experimental Section

### Materials and Synthesis

Elemental potassium (*Acros Organics*, 98%), sulfur (*abcr*, 99%), selenium (*Onyxmet*, 99.5%), iron (*Sigma-Aldrich*, 99%), and FeS (*Sigma-Aldrich*, 99%) were purchased commercially and used with-out further purification. Pyridine was dried over CaH$_2$ and freshly distilled prior usage. All preparation and manipulation steps were conducted inside a glovebox filled with argon, and/or under argon by using standard Schlenk techniques.

**EurJIC**
European Journal of Inorganic Chemistry

Research Article
doi.org/10.1002/ejic.202400522

**Chemistry Europe**
European Chemical
Societies Publishing

K$_2$S and K$_2$Se were synthesized by reacting potassium and sulfur(/ selenium) with the K:S(Se) ratio of 2:1 in liquid ammonia, according to the already reported protocol.[28] To synthesize **1** (688.03 g mol$^{-1}$), the stoichiometric ratio of K$_2$S (4.5 eq., 65.38 mmol, 7.208 g), FeS (2 eq., 29.06 mmol, 2.554 g), and elemental sulfur (0.5 eq., 7.26 mmol, 0.232 g) were mixed homogeneously, placed in a fused silica ampule, and heat treated using an oxygen-methane torch flame up to around 1200 K for around 10 minutes, followed by cooling down to room temperature. **2** (1016.29 g mol$^{-1}$) was synthesized in a same way by mixing the stoichiometric ratio of K$_2$Se (4.5 eq., 44.23 mmol, 6.951 g), iron (2 eq., 19.66 mmol, 1.098 g), and selenium (2.5 eq., 24.57 mmol, 1.940 g). After the heat treatment, the ampules were carefully broken, and the crude products were manually extracted to yield 9.41 g (94%) of dark red powder of **1** and 9.15 g (91%) of shiny dark brown powder of **2**, respectively. To obtain single crystals suitable for X-ray analysis, approx. 120 mg of the as-obtained products were placed in a 10 mL solvothermal glass vial with a pressure release cap, and 2 mL of pyridine as a solvent. The mixture was heat treated at 423 K for 48 hours and allowed to cool to room temperature.

### Characterization

Single crystals for **2** were isolated under an optical microscope, mounted in mineral oil (*STP Oil Treatment*), and stored in liquid nitrogen according to reported procedure.[29] A suitable crystal was investigated using a *Bruker D8 Venture* diffractometer with Mo-K$_\alpha$ radiation ($\lambda = 0.71073$ Å) at 100(1) K. The crystal structure was solved and refined in *Olex2*[30] using *ShelXT*[31] and *ShelXL*,[32] respectively. All structures were depicted using *DIAMOND4.5.2*.[33] The phase purity of the compounds was studied using a powder XRD (*Malvern Panalytical Empyrean*) using Cu-K$_\alpha$ radiation ($\lambda = 1.54184$ Å) at 293 K, whilst the samples were preparing by placing around 50 mg fine powder on the self 3D-printed polylactic acid holders.[29] The Rietveld structure refinements were carried out using *GSAS II*.[34] Details of the refinement parameters are available in the SI. The elemental analyses were conducted based on the EDX method using a *Zeiss Sigma 300VP* field emission scanning electron microscope (FE-SEM), coupled with two *Bruker, Quantax Xflash 6*, 60 mm$^2$, SSD, EDX detectors. Further details of the EDX measurements are provided in the SI.

The optical properties of **1** and **2** were measured using a UV-visible spectrometer (*Varian Cary 5000)* by recording the optical reflection spectra in the wavelength range of 200 to 1400 nm with the help of a *Praying Mantis™* accessory. Tauc plots were calculated to estimate the optical band gap energies. To measure dielectric and impedance properties, bulk samples were prepared by pressing around 400 mg of fine powder for each sample (pellet dimensions: Diameter of 13 mm and thickness of 3 mm) and sintered at 723 K for 18 hours. Both surface sides of the sintered pellets were covered by a layer of conductive adhesive silver paste (*abcr*, sheet resistivity $< 3.8 \times 10^{-3}$ $\Omega$ cm$^{-1}$, for the layer thickness of $3.8 \times 10^{-4}$ cm) as electrodes and cured at around 373 K for an hour. The dielectric measurements were conducted at room temperature in the frequency range of 20 Hz to 1 MHz using a precision LCR meter (*SOURCETRONIC*, ST2829 C) by applying a measurement voltage of 1 V without any bias voltage. The electrochemical impedance properties were measured at room temperature in the frequency range of 100 mHz to 1 MHz using an electrochemical impedance analyzer (EIS, *BioLogic* MTZ-35) by applying a measurement voltage of 100 mV.

## Supporting Information Summary

Further details about the single crystal XRD including the refinement and structural parameters, Rietveld structure refinement, and the EDX measurements are provided in the SI. The authors have cited an additional reference within the Supporting Information (Ref. [35]).

## Conflict of Interests

The authors declare no conflict of interest.

## Data Availability Statement

The data that support the findings of this study are openly available in ICSD at http://www2.fiz-karlsruhe.de/icsd home.html, reference number 2376648.

**Keywords:** Metalate · Solid-state synthesis · UV-Visible spectroscopy · Band gap · Crystal structure

[1] S. T. McBeath, Y. Zhang, M. R. Hoffmann, *Environ. Sci. Technol.* **2023**, *57*, 18700–18709.
[2] M. Keilwerth, W. Mao, M. Malischewski, S. A. V. Jannuzzi, K. Breitwieser, F. W. Heinemann, A. Scheurer, S. DeBeer, D. Munz, E. Bill, K. Meyer, *Nat. Chem.* **2024**, *16*, 514–520.
[3] P. Stüble, A. Berroth, C. Röhr, *Z. Naturforsch. B* **2016**, *71*, 485–501.
[4] M. R. Ghazanfari, A. Santhosh, J. C. Vrijmoed, K. Siemensmeyerd, B. Peterse, S. Dehnen, P. Jerabek, G. Thiele, *RSC Adv.* **2022**, *12*, 30514–30521.
[5] M. R. Ghazanfari, M. Kashefi, M. R. Jaafari, *J. Magn. Magn. Mater.* **2016**, *409*, 134–142.
[6] M. R. Ghazanfari, S. F. Shams, M. R. Jaafari, M. Kashefi, *Ceram. Int.* **2019**, *45*, 6030–6036.
[7] K. K. Kefeni, T. A. M. Msagati, B. B. Mamba, *Mater. Sci. Eng. B* **2017**, *215*, 37–55.
[8] A. Möller, *Z. Anorg. Allg. Chem.* **2001**, *627*, 2537–2541.
[9] W. Bronger, H. S. Genin, P. Müller, *Z. Anorg. Allg. Chem.* **1999**, *625*, 274–278.
[10] K. Klepp, H. Boller, *Monatsh. Chem.* **1981**, *112*, 83–89.
[11] J. M. Caron, J. R. Neilson, D. C. Miller, K. Arpino, A. Llobet, T. M. McQueen, *Phys. Rev. B* **2012**, *85*, 180405(R).
[12] W. Bronger, U. Ruschewitz, *J. Alloys Compd.* **1993**, *197*, 83–86.
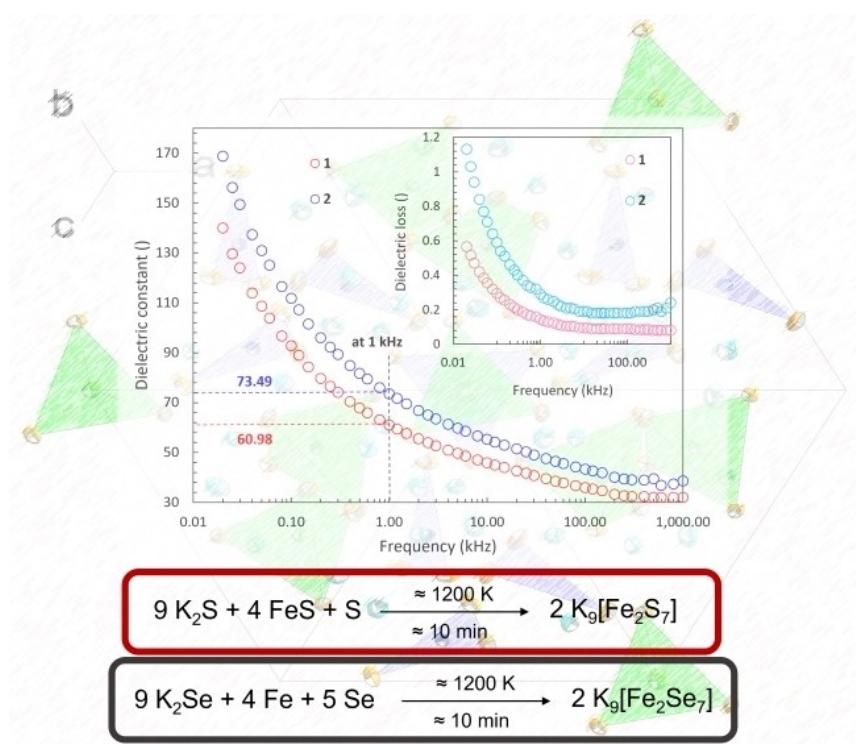[13] A. A. Kokhanovsky, *J. Phys. D* **2007**, *40*, 2210–2216.

[14] W. Bao, G. N. Li, Q. Z. Huang, G. F. Chen, J. B. He, D. M. Wang, M. A. Green, Y. M. Qiu, J. L. Luo, M. M. Wu, *Chin. Phys. Lett.* **2013**, *30*, 027402.

[15] R. Mahani, E. A. El-Sayad, *J. Adv. Dielectr.* **2019**, *9*, 1950001.

[16] Y. Dong, R. Zhu, Y. Jia, *J. Phys. Chem. C* **2021**, *125*, 14883–14890.

[17] G. Han, I. W. Yeu, K. H. Ye, S.-C. Lee, C. S. Hwang, J.-H. Choi, *J. Mater. Chem. C* **2021**, *9*, 851–859.

[18] V. Narendar, *Silicon* **2018**, *10*, 2419–2429.

[19] A. K. Bain, P. Chand, *Ferroelectrics: Principles and Applications*, First Edition, Wiley-VCH Verlag GmbH **2017**, pp. 6–22.

[20] P. Wu, M. Zhang, H. Wang, H. Tang, P. Bass, L. Zhang, *AIP Adv.* **2017**, *7*, 075210.

[21] M. R. Ghazanfari, K. Siemensmeyer, A. Santhosh, J. C. Vrijmoed, M. Tallu, S. Dehnen, P. Jerabek, G. Thiele, *Inorg. Chem.* **2023**, *62*, 38.

[22] J. Jamnik, J. Maier, *Phys. Chem. Chem. Phys.* **2001**, *3*, 1668–1678.

[23] Z. Osman, M. I. Mohd Ghazali, L. Othman, K. B. Md Isa, *Results Phys.* **2012**, *2*, 1.

[24] S. Susarla, A. B. Puthirath, T. Tsafack, D. Salpekar, G. Babu, P. M. Ajayan, *ACS Appl. Mater. Interfaces* **2020**, *12*, 1005–1013.

[25] F. Meutzner, M. Zschornak, A. A. Kabanov, T. Nestler, T. Leisegang, V. A. Blatov, D. C. Meyer, *Chem. Eur. J.* **2019**, *25*, 8623–8629.

[26] R. Schlem, M. Ghidiu, P. Culver, A.-L. Hansen, W. G. Zeier, *ACS Appl. Energ. Mater.* **2020**, *3*, 9–18.

[27] M. R. Ghazanfari, A. Santhosh, K. Siemensmeyer, F. Fuß, L. Staab, J. C. Vrijmoed, B. Peters, M. Liesegang, S. Dehnen, O. Oeckler, P. Jerabek, G. Thiele, *Adv. Electron. Mater.* **2022**, *8*, 2200483.

[28] G. W. Watt, *Chem. Rev.* **1950**, *46*, 289–315.

[29] F. Fuß, M. Rieckert, S. Steinhauer, M. Liesegang, G. Thiele, *J. Appl. Crystallogr.* **2022**, *55*, 686–692.

[30] O. V. Dolomanov, L. J. Bourhis, R. J. Gildea, J. A. K. Howard, H. Puschmann, *J. Appl. Crystallogr.* **2009**, *42*, 339–341.

[31] G. M. Sheldrick, *Acta Crystallogr. Sect. A* **2015**, *71*, 3–8.

[32] G. M. Sheldrick, *Acta Crystallogr. Sect. C* **2015**, *71*, 3–8.

[33] K. Brandenburg, *DIAMOND (4.6.4)*, Crystal Impact GbR, Bonn, **2020**.

[34] B. H. Toby, B. H. R. B. von Dreele, *J. Appl. Crystallogr.* **2013**, *46*, 544–549.

[35] G. M. Sheldrick, *SADABS v. 2: Multi-Scan Absorption Correction*, Bruker-AXS, WA **2012**.

# RESEARCH ARTICLE

*Dr. M. Reza Ghazanfari, M. Sc. L. Janus,*
*M. Sc. I. Ramadan, M. Sc. M. Tallu,*
*Prof. Dr. S. Dehnen, Dr. G. Thiele\**

1 – 10

**Semiconducting Mixed Valence Sulfido (Selenido) Ferrates: Optical, Dielectric, and Electrochemical Impedance Properties**

Mixed valence, isotypic $K_9[Fe_2S_7]$ and $K_9[Fe_2Se_7]$ were synthesized through a straightforward, large-scale method. The optical and electrical measurements indicate semiconductivity with low ionic conductivities and surprisingly high dielectric constants.